October 2000

Control of High-Harmonic Generation and Laser-Assisted X-ray-Atom Scattering with Static Electric and Magnetic Fields

D. B. Milošević
Max-Born-Institut, Berlin, and University of Sarajevo

Anthony F. Starace
University of Nebraska-Lincoln, astarace1@unl.edu

Laser Physics, Vol. 10, No. 1, 2000, pp. 278–293.

Control of High-Harmonic Generation and Laser-Assisted X-ray-Atom Scattering with Static Electric and Magnetic Fields

D. B. Milošević* and A. F. Starace**

* *Max-Born-Institut, Max-Born-Strasse 2a, Berlin, 12489 Germany, and Faculty of Science and Mathematics, Department of Physics, University of Sarajevo, Zmaja od Bosne 35, Sarajevo, 71000 Bosnia and Herzegovina*
e-mail: milos@mbi-berlin.de

** *Department of Physics and Astronomy, The University of Nebraska, 116 Brace Laboratory, Lincoln, Nebraska 68588-0111, USA*
e-mail: astarace1@unl.edu

Received July 6, 1999

Abstract—We consider the use of strong static fields to control two related atomic processes: laser-assisted x-ray-atom scattering (XAS) and high-harmonic generation (HHG). We first analyze the laser field intensity dependence of the differential cross section (DCS) plateau structures for the laser-assisted XAS process in the presence of a static electric field as a function of the number of photons exchanged with the laser field. Besides the recently discovered (Milošević, D.B. and Starace, A.F., 1998, *Phys. Rev. Lett.*, **81**, 5097) extended plateau for absorbed photons, which indicates a substantial increase of the scattered x-ray energies, a new plateau, having many orders of magnitude larger DCS, appears for higher laser field intensities. We show furthermore a connection between this process and HHG. We also consider control of HHG with static electric and magnetic fields which are parallel to the laser polarization. The B field can considerably increase the harmonic emission rate (Milošević, D.B. and Starace, A.F., 1999, *Phys. Rev. Lett.*, **82**, 2653). The rate of a chosen harmonic is maximal whenever an integer multiple of the cyclotron period of the electron's motion perpendicular to the magnetic field is equal to the return time to the nucleus of the laser-field-generated electron wave packet in the intermediate state. While the B field has only a modest effect on the plateau cutoff positions, the static electric field can introduce additional plateaus and cutoffs. A properly chosen combination of static E and B fields can increase both the emission rate and the maximum harmonic order. The locations and magnitudes of the plateaus, both for XAS and HHG, are explained using the classical three-step model.

I. INTRODUCTION

Over the past decade high-harmonic generation (HHG) in laser-irradiated atomic gases has been extensively studied [1]. Many efforts have been made in order to control HHG, especially due to the potentially important applications of the coherent soft x-rays that might be produced via HHG [2]. It is known that the harmonic output can be manipulated by changing the driving field or altering the medium which generates harmonics. For example, a bichromatic driving laser field provides two additional parameters for control of HHG: the relative intensity and the relative phase of the fields [3, 4]. Polarization of the laser field [4, 5], as well as the shape of the laser pulse [6], are also parameters suitable for such control. For ultra-short pulses, the initial laser field phase has a significant influence on the HHG process [6]. The HHG process can also be controlled by adding a static electric field [7–9] or a static magnetic field [10, 11] to the driving laser field. The usual media used in HHG are atomic gases, but HHG has also been examined for ions [12], molecular gases [13, 14], and atomic clusters [15]. In addition, control of HHG has been explored theoretically for the case of an initial state prepared as a coherent superposition of states [16]. In the present paper we consider the control of HHG by adding parallel static electric and magnetic fields.

Recently, another process which enables generation of coherent soft x-rays—laser-assisted x-ray-atom scattering (XAS)—was proposed [17, 18]. It was shown [18] that, by controlling the laser-assisted XAS process with a strong static electric field, it is possible to generate coherent x-ray photons with energies in the "water window" (between the K-shell absorption edges of carbon (284 eV, 4.37 nm) and oxygen (532 eV, 2.33 nm)). Coherent x-rays in this energy region would have important applications to imaging living biological structures by means of x-ray holography [2]. In the present paper we further analyze laser-assisted XAS both in the presence and in the absence of a static electric field. In the next two sections we show how this process is related to HHG and how both processes can be understood using a simple three-step physical model and a classical analysis. In Section IV we present our quantum-mechanical theory and numerical results for the laser-assisted XAS process and connect these results with the classical results of Section III. In Section V we present our results for HHG in the presence of static electric and magnetic fields. Finally, Section VI presents our conclusions.

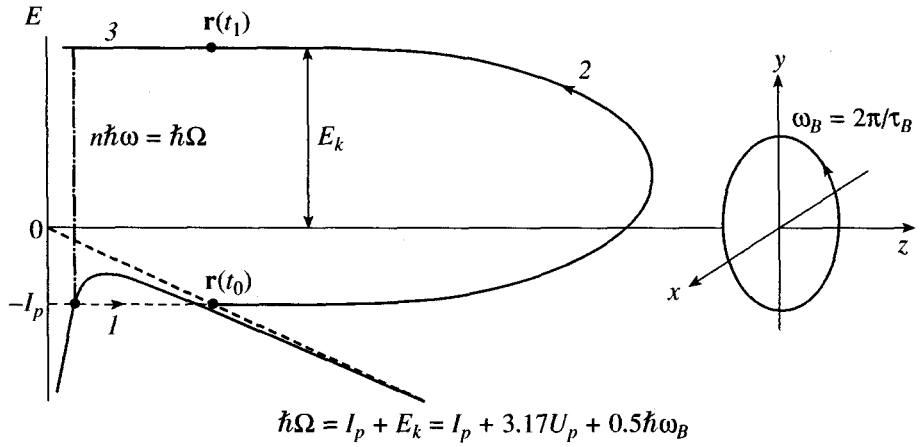

Fig. 1. Schematic of high-harmonic generation in the presence of a magnetic field. The laser field is linearly polarized along the z-axis. Numbers 1, 2, and 3 denote the steps of the three-step model. The E-axis denotes the electron energy coordinate, and ω_B is the cyclotron frequency for the electron's (perpendicular) motion in the xy-plane. See the text for a more detailed explanation.

II. THREE-STEP MODEL

The main characteristics of both the HHG and laser-assisted XAS processes can be explained using the so-called "three-step" physical model [19]. According to this model, the first step is the ionization of an atomic electron, while the second step is the propagation of a free electron in the laser field. The third step is the collision between the electron, driven back by the laser field, and the atomic core, whereupon the electron recombines, emitting a harmonic or x-ray photon. This model is schematically presented in Fig. 1 for the HHG process. The above-mentioned steps are denoted by the numbers 1, 2, and 3, respectively, in Fig. 1. The atom, having the ionization energy I_p, is in its ground state when the laser field switches on. The atomic potential is lowered by the influence of the laser field, and the atom can be ionized (either by tunnelling or by multiphoton ionization). The electron is "born" at the point $\mathbf{r}(t_0)$ with the velocity $\mathbf{v}_0$ (where both are usually assumed equal to zero). The free electron propagates in the laser field and acquires an energy E_k. When the electron is back at the origin ($\mathbf{r}(t_1) = \mathbf{r}(t_0)$), it can then recombine, emitting a harmonic photon having energy $\hbar\Omega = I_p + E_k$. The HHG spectrum forms an extended plateau which consists of many harmonics with comparable intensities. The maximum kinetic energy which an electron can acquire from a linearly polarized laser field is $3.17U_p$, where $U_p = e^2E_L^2/(4m\omega^2)$ is the ponderomotive energy, where $-e$ and m are the electron charge and mass, and where E_L and ω are the laser electric field amplitude and frequency, respectively. (We will use here SI units.) This result gives the well-known cutoff law for HHG: $\hbar\Omega_{max} = I_p + 3.17U_p$ [19, 20]. If an additional parallel static magnetic field B is present (as in Fig. 1), then the harmonic photon energy should be increased by the ground-state Landau level energy $\hbar\omega_B/2 = e\hbar B/(2m)$, where ω_B is the cyclotron frequency for the electron's perpendicular motion [11]. The above-mentioned appearance of a plateau with its cutoff is in agreement with more rigorous quantum-mechanical calculations [1, 20].

In Fig. 2 we present a similar schematic for laser-assisted XAS. The laser-field-lowered atomic potential is now shifted by the incident x-ray photon energy $\hbar\omega_K$. If $\hbar\omega_K > I_p$, then the electron can be born at the point $z(t_0)$ with the initial velocity $\mathbf{v}_0$, where $m v_0^2/2 = \hbar\omega_K - I_p$. During the second step—laser-field driven propagation—the electron exchanges an energy $n\hbar\omega$ with the laser field. The third step is the same as for HHG: the electron, having kinetic energy E_k, recombines at the point $z(t_1) = z(t_0)$, emitting an x-ray with the energy $\hbar\omega_{K'} = E_k + I_p = \hbar\omega_K + n\hbar\omega$. For $n > 0$ the electron absorbs from the laser field an energy proportional to U_p ($n\hbar\omega = cU_p$, see the solid line denoted by 2 in Fig. 2). This process corresponds to a positive n plateau of the differential cross section (DCS) for laser-assisted XAS (see Section IV). The maximum value of c is different from the corresponding HHG value $c = 3.17$ and will be determined in the next section. For $n < 0$, stimulated emission of photons occurs, and the scattered x-ray photon energy is lower. It was shown [17] that this process corresponds to a negative n DCS plateau and that recombination is most probable for $E_k = 0$, so that the most probable number of emitted photons is given by $n\hbar\omega = I_p - \hbar\omega_K$ (see the dotted 2' line in Fig. 2). The DCS cutoff position for negative values of n is determined by the energy conserving condition: $\hbar\omega_{K'} = \hbar\omega_K + n\hbar\omega \geq 0$, which gives $n \geq -\omega_K/\omega$.

III. CLASSICAL ANALYSIS

In this section we analyze the above-described three-step model for HHG and laser-assisted XAS quantitatively using a classical analysis. The electron is assumed to be born at time t_0 at the origin $\mathbf{r}(t_0) = \mathbf{0}$ with the velocity $\mathbf{v}(t_0) = \mathbf{v}_0$, where $v_0 = 0$ for HHG and

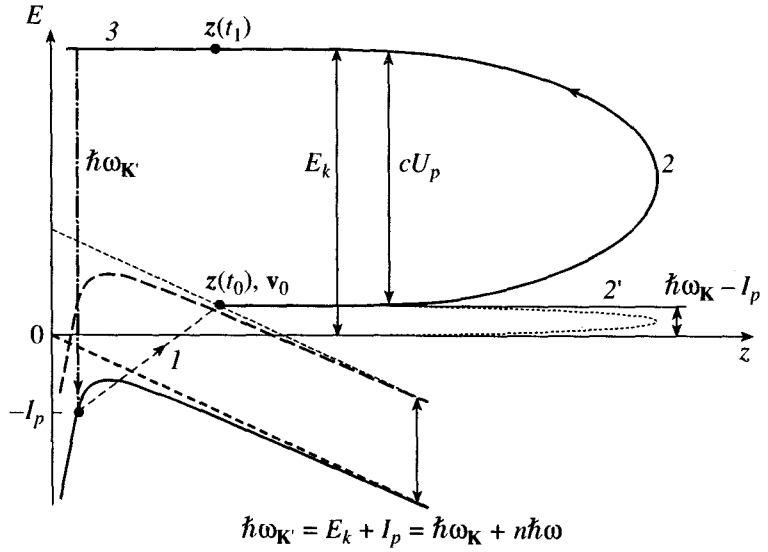

Fig. 2. Schematic of laser-assisted x-ray-atom scattering, presented similarly to Fig. 1. The combined atomic and electric field potential is shifted by the incident x-ray photon energy $\hbar\omega_K$. The electron propagation step of the three-step model is denoted by 2 (2') for the process in which a positive (negative) n plateau is formed.

$m v_0^2/2 = \hbar\omega_K - I_p$ for laser-assisted XAS. This electron then moves under the influence of the laser field $\mathbf{E}_L(t)$ and the static fields $\mathbf{E}_S$ and $\mathbf{B}$, if they are present. Solving Newton's equation for the electron, $m\ddot{\mathbf{r}} = -e[\mathbf{E}_L(t) + \mathbf{E}_S + \dot{\mathbf{r}} \times \mathbf{B}]$, one obtains the electron kinetic energy E_k at the time t_1 when the electron returns to the origin. The maximum of this energy is determined by two conditions: $\mathbf{r}(t_1) = 0$ (this is the condition that the electron, after the return time $\tau = t_1 - t_0$, comes back to the atomic core) and $\partial E_k/\partial t_0 = 0$ (this condition determines the optimum time t_0, at which the electron is born, for which E_k has maximum). In the case of a linearly polarized laser field and parallel static fields, Newton's equation separates, so that: $m\dot{x} = eBy$, $m\dot{y} = -eBx$, and $m\dot{z} = e[A_L(t) + A_S(t) - A_L(t_0) - A_S(t_0)] + mv_0$, where $\mathbf{A}_j(t) = -\int^t dt' \mathbf{E}_j(t')$, $j = L, S$. Thus, $E_k = m\dot{\mathbf{r}}^2(t)/2 = e^2\{[A_L(t) + A_S(t) - A_L(t_0) - A_S(t_0) + (m/e)v_0]^2 + B^2(x^2 + y^2)\}/(2m)$. In the presence of a magnetic field, the electron rotates in the plane perpendicular to the magnetic field direction with the cyclotron period $\tau_B = 2\pi/\omega_B$, while its parallel motion is determined by the laser field and the static electric field. The electron returns to the origin at time $t_1 = t_0 + \tau_B, t_0 + 2\tau_B, \ldots$, if the condition $z(t_1) = 0$ is fulfilled. This condition leads to

$$\int_{t_0}^{t_1} dt[A_L(t) + A_S(t)] = \left[A_L(t_0) + A_S(t_0) - \frac{m}{e}v_0\right](t_1 - t_0). \quad (1)$$

For a laser field defined by $\mathbf{E}_L(t) = E_L \sin\omega t\,\hat{\mathbf{z}}$, we introduce the notation

$$\varphi = \omega t_1, \quad \sigma = \frac{\omega\tau}{2}, \quad a(\sigma) = \sin\sigma,$$
$$b(\sigma) = \cos\sigma - \frac{\sin\sigma}{\sigma}, \quad c(\sigma) = \frac{mv_0\omega}{eE_L} - \frac{E_S}{E_L}\sigma, \quad (2)$$

whereupon (1) can be rewritten as

$$a(\sigma)\sin(\varphi - \sigma) + b(\sigma)\cos(\varphi - \sigma) = c(\sigma), \quad (3)$$

and the electron's kinetic energy becomes

$$E_k = 8U_p\left[a(\sigma)\sin(\varphi - \sigma) - c(\sigma) + \frac{mv_0\omega}{2eE_L}\right]^2. \quad (4)$$

Equation (3) can be rewritten as a quadratic equation in the variable $X = \sin(\varphi - \sigma)$, and, therefore, for each τ we have two solutions for X:

$$X(\sigma) = \frac{1}{a^2 + b^2}[ac \pm b(a^2 + b^2 - c^2)^{1/2}]. \quad (5)$$

Introducing these solutions into (4), we obtain the electron kinetic energy as a function of the return time $\tau = 2\sigma/\omega$. The maximum of this energy can be obtained from the stationary kinetic energy condition $\partial E_k/\partial t_0 = 0$ (for more details see [8] for HHG, and [18] for laser-assisted XAS). The two solutions in (5) correspond to positive and negative values of $E_L(t)$ at the moment of ionization. For one solution $\mathbf{E}_L(t_0)$ is parallel to the static electric field $\mathbf{E}_S$, while for the other it is antiparallel. In absence of the static electric field and for the HHG process (zero initial velocity), these two solutions coincide. In this case, $c(\sigma) = 0$ and there is only one solution: $E_k = 8a^2b^2U_p/(a^2 + b^2)$. For laser-assisted XAS

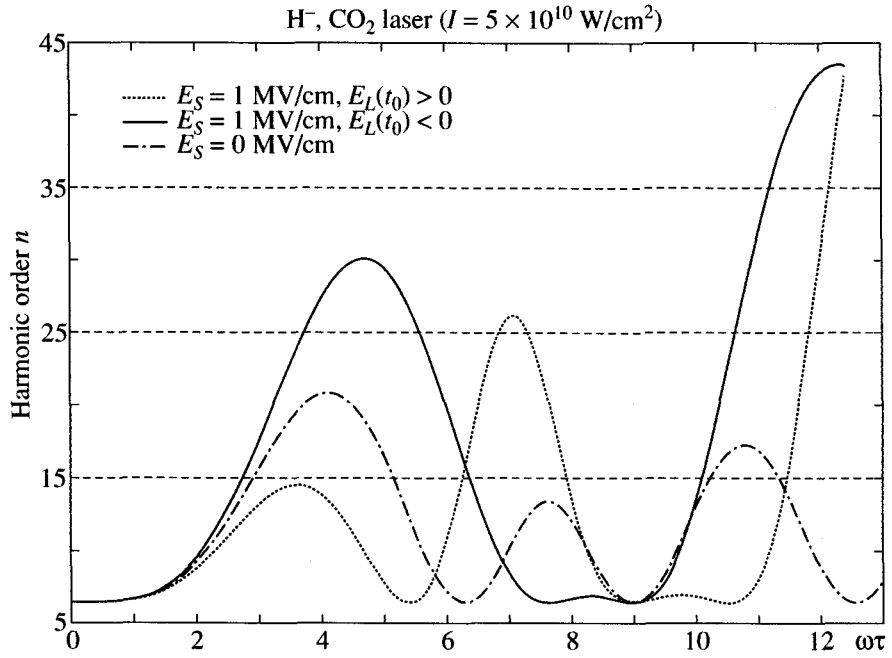

Fig. 3. Harmonic order n as an oscillatory function of the dimensionless variable $\omega\tau$ for the H^- ion in a CO_2 laser with intensity $I = 5 \times 10^{10}$ W/cm^2, and with (full and dotted lines) or without (dot-dashed line) a parallel static electric field having strength $E_S = 1$ MV/cm. τ is the classical electron return time to the origin under the influence of both electric fields. The full (dotted) curves correspond to parallel (antiparallel) static and laser fields at $t = t_0$.

(nonzero electron initial velocity), the energy exchanged with the laser field is

$$n\hbar\omega = E_k - \frac{mv_0^2}{2} = 8U_p[a(\sigma)X(\sigma) - c(\sigma)] \times \left[a(\sigma)X(\sigma) + \frac{E_S}{E_L}\sigma\right], \quad (6)$$

which has two solutions whenever (5) gives nondegenerate solutions for $X(\sigma)$.

Let us analyze in more detail the above solutions for HHG in the presence of a static electric field. In Fig. 3 we present the harmonic order $n(\omega\tau) = (I_p + E_k)/\hbar\omega$ as a function of the dimensionless parameter $\omega\tau$ for the H^- ion (having electron affinity $I_p = 0.754$ eV), a CO_2 laser ($\hbar\omega = 0.1165$ eV) with intensity $I = 5 \times 10^{10}$ W/cm^2, and a static electric field with strength $E_S = 1$ MV/cm. We present the two solutions for n by a solid curve for the parallel orientation of $\mathbf{E}_L(t_0)$ and $\mathbf{E}_S$, and by a dotted curve for the antiparallel orientation. For a long enough return time ($\omega\tau > 12.41$ in the present case), the laser field cannot return the electron back to the nucleus because the influence of the static electric field, which is proportional to the return time, becomes too large. The maxima of the curves presented explain why the cutoffs of the harmonic spectrum which we obtain in our quantum-mechanical calculations (cf. Section V) appear at $n = 31$ and 43. For comparison, we also present, by a dot-dashed curve, the results obtained in the absence of the static electric field. In this case, there is no upper limit for $\omega\tau$. The maximum value $n_{max} = 21$ corresponds to the cutoff law $n_{max}\hbar\omega = I_p + 3.17U_p$.

For the laser-assisted XAS process, in absence of a static electric field, there are no real solutions of (3)–(6) if the initial electron kinetic energy $mv_0^2/2 = \hbar\omega_K - I_p$ is larger than the maximum energy which the electron can acquire in the laser field. In this case, the laser field alone is not strong enough to return the electron to the nucleus, and, therefore, it is not capable of producing a positive n plateau. But, in the presence of a static electric field parallel to $\mathbf{v}_0$, the electron can be returned to the nucleus because the static field acts on it with the force $-eE_S\hat{\mathbf{z}}$. In this case, the energy which the electron acquires from the laser field can be much larger than $3.17U_p$. In order to illustrate this, in Fig. 4 we present the solutions for the energy exchanged with the laser field, (6), in units of U_p, as functions of $\omega\tau$ for H atoms ($I_p = 13.6$ eV), a Nd : YAG laser ($\hbar\omega = 1.17$ eV), and a static electric field with strength $E_S = 20$ MV/cm. (This large value of E_S is chosen to reduce the number of oscillations in Fig. 4, thereby allowing a clearer picture of our physical interpretation than would be the case for smaller values of E_S.) The incident x-ray photon energy is $\hbar\omega_K = 31\hbar\omega$, and we consider two values of the laser field intensity. For the lower laser field intensity, $I = 4 \times 10^{13}$ W/cm^2, there are no solutions for $\omega\tau < 10$ and $\omega\tau > 45.5$. For $\omega\tau < 10$ the influence of the static field, which increases with the increase of the return time τ, is not yet strong enough to

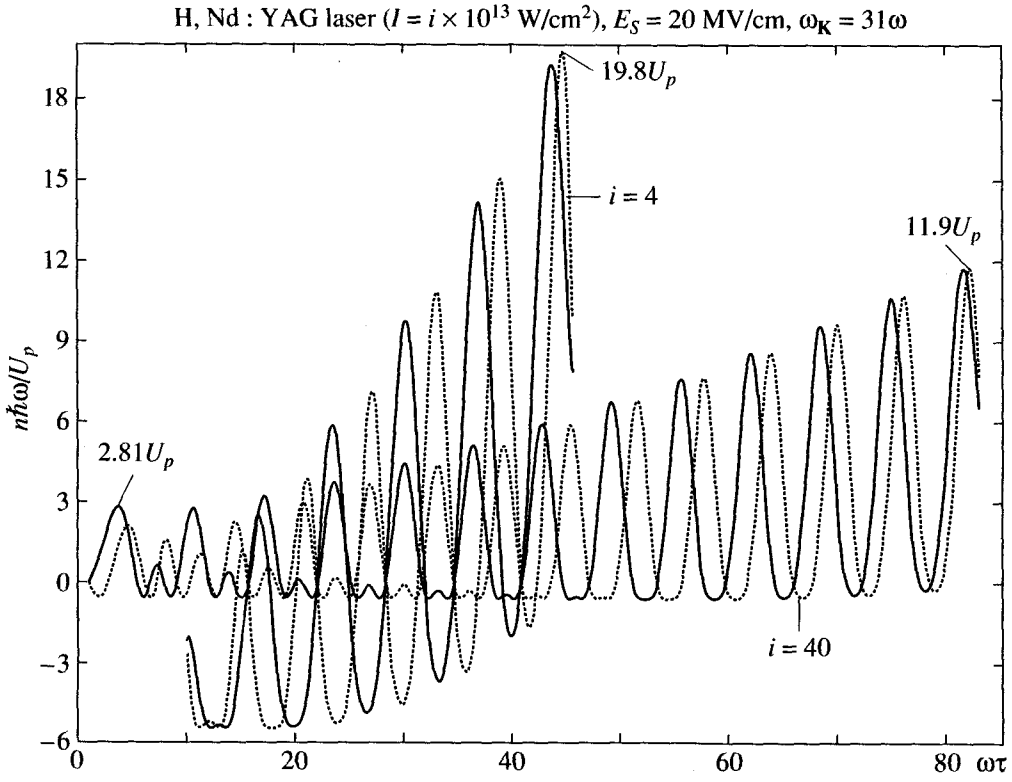

Fig. 4. Energy exchanged with the laser field in laser-assisted x-ray-hydrogen atom scattering, in units of the ponderomotive energy, as a function of the electron return time τ (multiplied by the laser frequency ω) for the case of a Nd : YAG laser and a static electric field having strength E_S = 20 MV/cm. The incident x-ray photon energy is $\hbar\omega_K = 31\hbar\omega$ and the laser field intensity is $I = 4 \times 10^{13}$ W/cm^2 and 4×10^{14} W/cm^2. The results are obtained as solutions of (6). The full (dotted) curves correspond to parallel (antiparallel) static and laser field at $t = t_0$.

support the laser-driven electron to overcome the initial electron kinetic energy and to return the electron to the origin. For $\omega\tau > 10$, solutions of (6) exist and can contribute to a positive n plateau of the DCS for laser-assisted XAS. However, for $\omega\tau > 45.5$ the influence of the static field is too strong, so that the laser field cannot return the electron to the origin. The absence of solutions for $\omega\tau > 45.5$ corresponds to the cutoff of the DCS at $19.8U_p$ for positive n. For higher laser field intensity, $I = 4 \times 10^{14}$ W/cm^2, solutions exist for $1 < \omega\tau < 82.8$. The solid curve in Fig. 4 has a maximum at $n_{\max,1}\hbar\omega = 2.81U_p$ during the first optical cycle ($0 < \omega\tau < 2\pi$). In Section IV we will see that this maximum gives the position of the first cutoff of the DCS as a function of the number of photons n exchanged with the laser field. The solutions for $I = 4 \times 10^{14}$ W/cm^2 and for higher values of $\omega\tau$ correspond to an extended positive n plateau, with its cutoff at $n_{\max,2}\hbar\omega = 11.9U_p$.

Let us now explore how the positions of these low- and high-energy cutoffs depend on the laser field intensity. In Fig. 5 we present results for $n_{\max}\hbar\omega/U_p$ as a function of the laser field intensity for three values of the incident x-ray photon energy: $\hbar\omega_K = 15\hbar\omega$, $31\hbar\omega$, and $61\hbar\omega$, and for two values of the ratio of the static and the laser field strengths: (a) 0.01 and (b) 0.1. One can see that, in the high laser field intensity limit, the cutoff positions behave as $n_{\max,1}\hbar\omega = c_a U_p$ and $n_{\max,2}\hbar\omega = d_a U_p$, where the asymptotic quantities c_a and d_a depend only on the ratio E_S/E_L. The values of c_a and d_a, shown in Fig. 5, are in excellent agreement with the values obtained in [8] for HHG with zero initial electron velocity. (Note that for intensities I with $n_{\max,1} < 0$ in Fig. 5, there is no plateau for laser-assisted XAS for $\hbar\omega_{K'} > \hbar\omega_K$.) It is important to note that $n_{\max,2}\hbar\omega/U_p$ approaches d_a from above, and that very high values of the scattered x-ray photon energies $\hbar\omega_{K'} > n_{\max,2}\hbar\omega + \hbar\omega_K$ can be obtained for relatively low laser field intensities. The quantity c_a decreases with decrease of E_S/E_L and, for $E_S = 0$, approaches the value 3.17, which is the cutoff value for the HHG process in absence of the static field. Therefore, we have established a connections between laser-assisted XAS and HHG.

IV. QUANTUM-MECHANICAL RESULTS FOR LASER-ASSISTED X-RAY-ATOM SCATTERING

Treatments of x-ray scattering in the absence of a laser field can be found in the textbooks by Heitler [21]

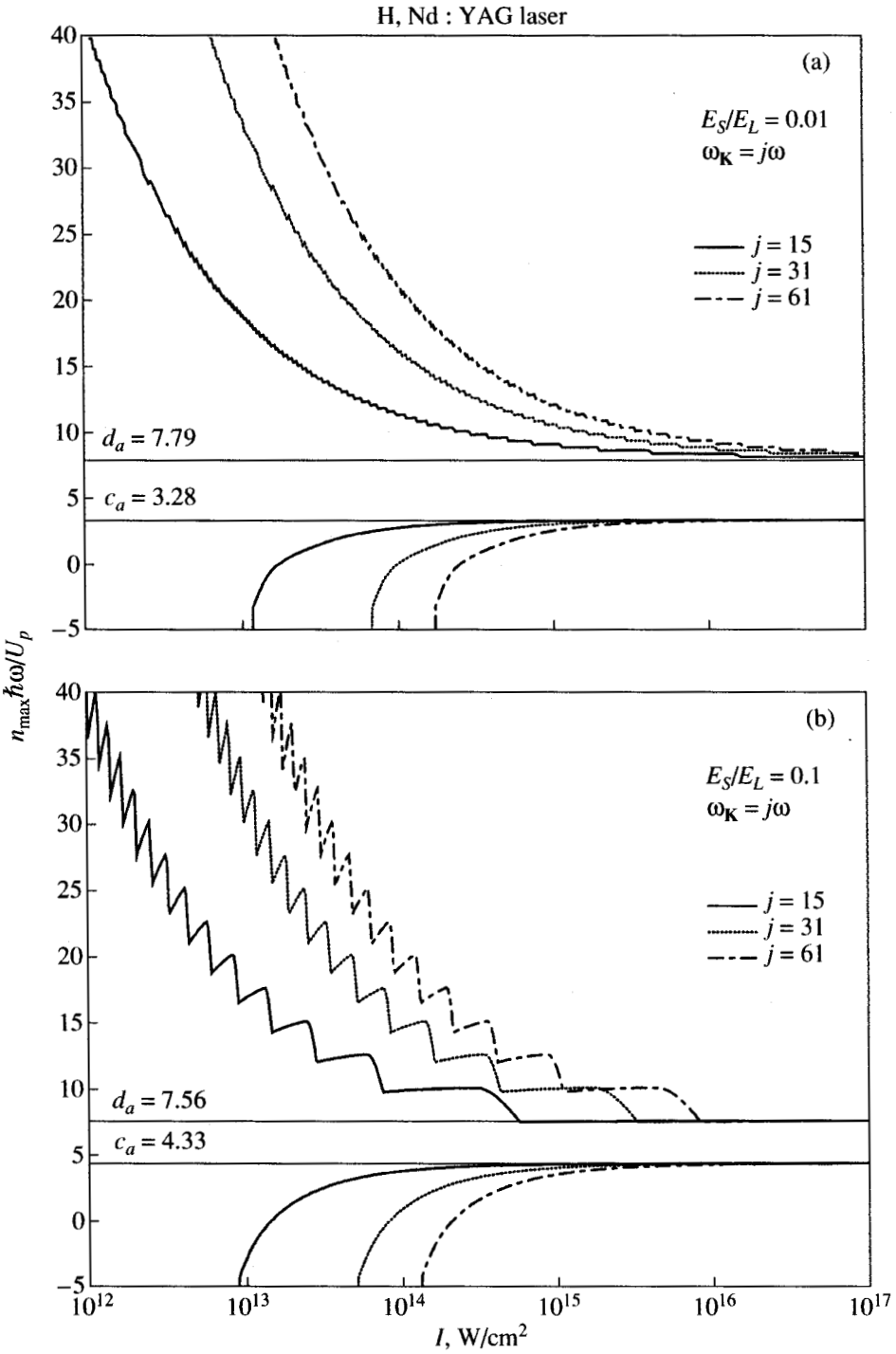

Fig. 5. Maximum energy exchanged with the laser field in laser-assisted x-ray-hydrogen atom scattering, in units of the ponderomotive energy, as a function of the laser field intensity, for three values of the incident x-ray photon energy $\hbar\omega_K = 15\hbar\omega$, $31\hbar\omega$, and $61\hbar\omega$, and for two values of the static and the laser electric field ratio: (a) $E_S/E_L = 0.01$ and (b) 0.1. The two asymptotic horizontal lines, denoted by c_a and d_a, correspond to the cutoff values of the HHG spectrum.

and by Loudon [22]. There are many papers in which x-ray scattering by bound systems is considered in the absence of the laser field. According to an early one by Levinger [23], one sees that this theory can be traced back to H.A. Bethe. As an example of more recent work, we cite the paper by Jung *et al.* [24]. The *S*-matrix theory of laser-assisted XAS was presented in [17]. A detailed derivation of the main expressions for

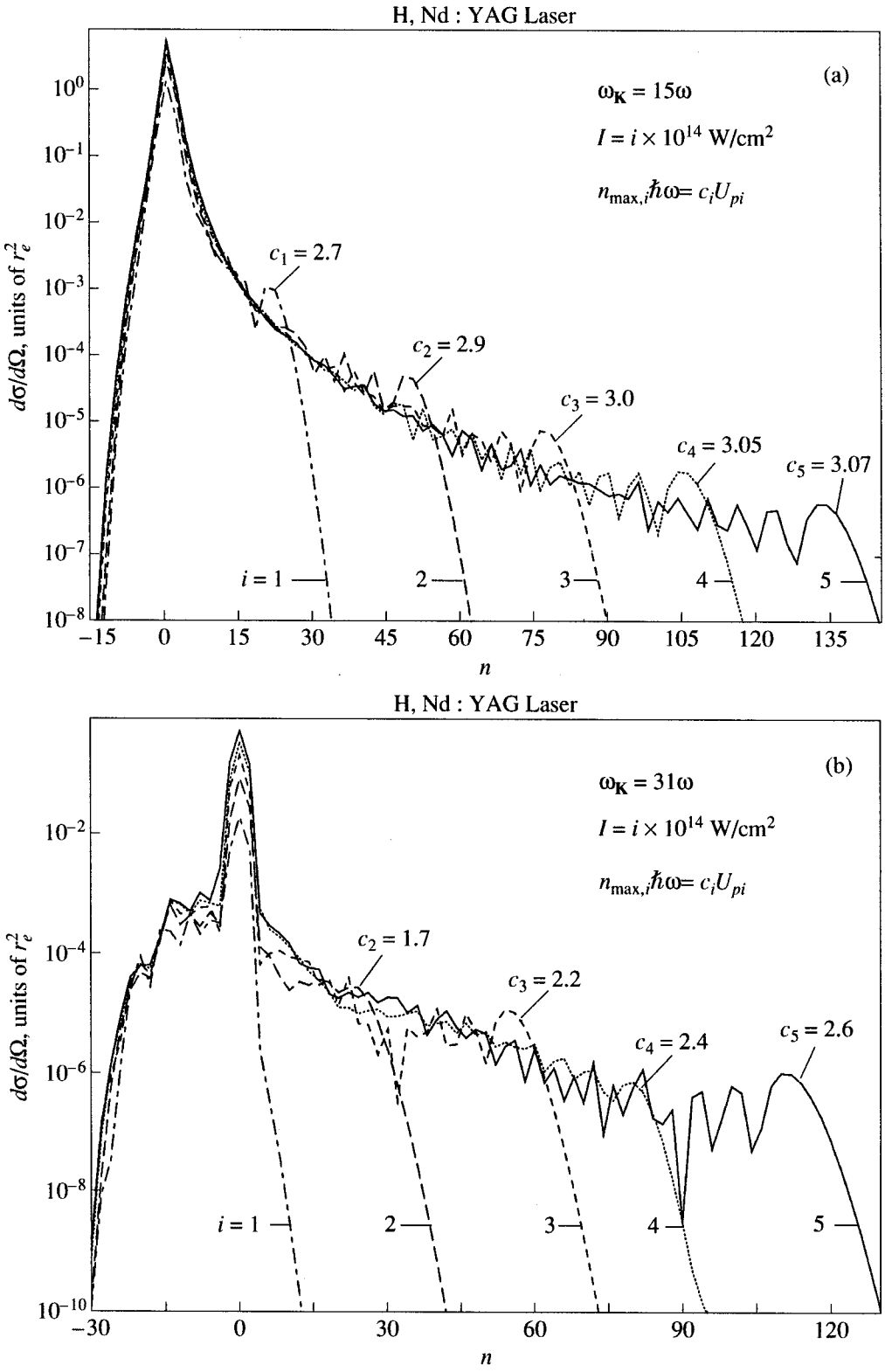

Fig. 6. The DCS for x-ray-hydrogen atom scattering in units of r_e^2 (where $r_e = 2.8 \times 10^{-15}$ m is the classical electron radius) as a function of the number n of absorbed ($n > 0$) or emitted ($n < 0$) laser field photons, for different laser field intensities $I(i) = i \times 10^{14}$ W/cm^2, where $i = 1$ (dot-dashed curve), 2 (long-dashed curve), 3 (dashed curve), 4 (dotted curve), and 5 (solid curve). The laser field is linearly polarized and monochromatic with photon energy $\hbar\omega = 1.17$ eV. The energy of the incident x-ray photons, $\hbar\omega_K$, is: (a) 15ω, (b) 31ω, and (c) 61ω. The energy cutoff positions are denoted by multiples c_i of the ponderomotive potential energy U_{pi} for laser field intensity $I(i)$.

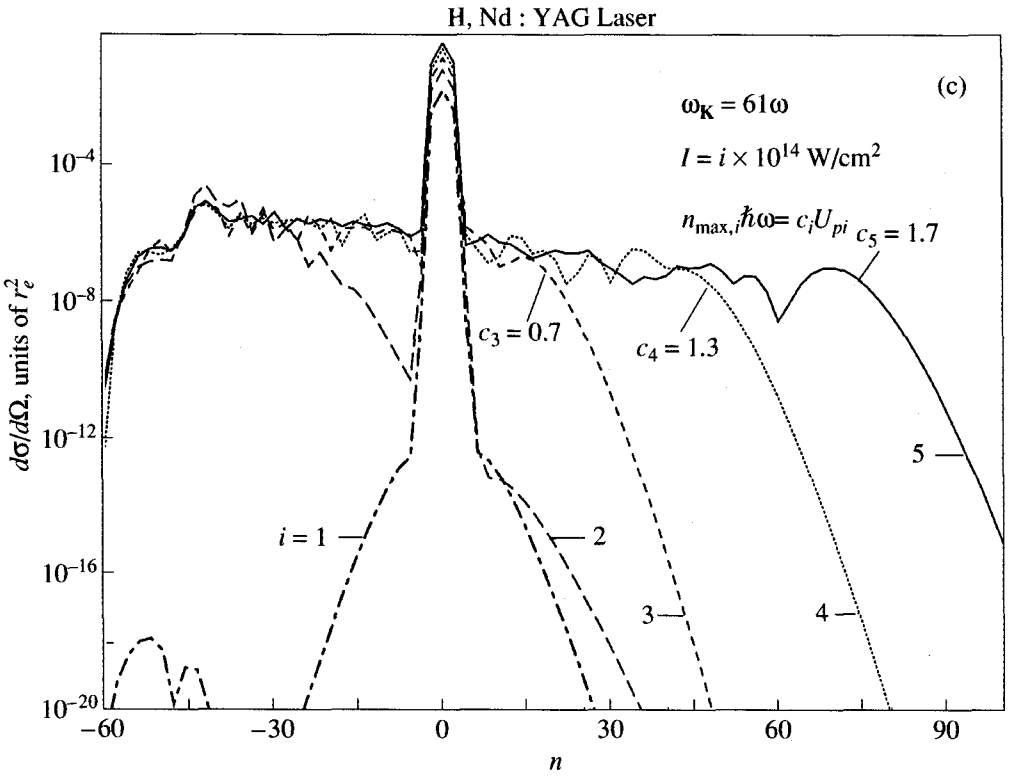

Fig. 6. (Contd.)

the DCS for laser-assisted XAS (including discussion of the approximations used) is presented in that paper and will not be repeated here. The final result for the DCS for laser-assisted XAS with absorption ($n > 0$) or emission ($n < 0$) of n laser photons having frequency ω is

$$\frac{d\sigma(n)}{d\Omega_{\hat{\mathbf{K}}'}} = \left(\frac{e^2}{4\pi\varepsilon_0\hbar}\right)^2 KK'^3\left|T^{(+)}_{\mathbf{K},\mathbf{K}'}(n) + T^{(-)}_{\mathbf{K}',\mathbf{K}}(n)\right|^2, \quad (7)$$

where $K = \omega_{\mathbf{K}}/c$, $K' = \omega_{\mathbf{K}'}/c$, and $\hbar\omega_{\mathbf{K}}$ and $\hbar\omega_{\mathbf{K}'} = \hbar\omega_{\mathbf{K}} + n\hbar\omega$ are the energies of the incident and scattered x-ray photons, respectively. The T-matrix elements,

$$T^{(\pm)}_{\mathbf{K},\mathbf{K}'}(n) = \int_0^{2\pi} \frac{d\varphi}{2\pi} \mathcal{T}^{(\pm)}_{\mathbf{K},\mathbf{K}'}(\varphi)\exp(in\varphi), \quad (8)$$

are the Fourier components of the matrix elements

$$\mathcal{T}^{(\pm)}_{\mathbf{K},\mathbf{K}'}(\varphi) = \int_0^{\infty} d\tau \int d\mathbf{q} \exp\{-i[S(\mathbf{q}; t, \tau)/\hbar \pm \omega_{\mathbf{K}'}\tau]\} \quad (9)$$
$$\times \left\langle \psi_0 | \mathbf{r}\cdot\hat{\mathbf{e}}_{\mathbf{K}} | \mathbf{q} + \frac{e}{\hbar}\mathbf{A}(t)\right\rangle \left\langle \mathbf{q} + \frac{e}{\hbar}\mathbf{A}(t-\tau) | \mathbf{r}\cdot\hat{\mathbf{e}}_{\mathbf{K}'} | \psi_0 \right\rangle,$$

where $|\psi_0\rangle$ is the atomic ground-state ket vector, $|\mathbf{q}\rangle$ is a plane-wave ket vector for the electron, $\varphi \equiv \omega t$, and $\hat{\mathbf{e}}_{\mathbf{K}}$ and $\hat{\mathbf{e}}_{\mathbf{K}'}$ are the unit polarization vectors of the incident and scattered photons, respectively (for simplicity, we assume parallel polarizations in all our numerical calculations). $\mathbf{A}(t)$ and $S(\mathbf{q}; t, \tau) = \int_{t-\tau}^{t} dt' \{[\hbar\mathbf{q} + e\mathbf{A}(t')]^2/(2m) + I_p\}$ are the vector potential and the electron's quasiclassical action in the presence of both a laser field and a static electric field. The matrix element $T^{(-)}_{\mathbf{K}',\mathbf{K}}(n)$ corresponds to the process in which an x-ray photon having wave vector $\mathbf{K}$ and energy $\hbar\omega_{\mathbf{K}}$ is absorbed first. The ionized electron propagates under the influence of both the laser and static electric fields during the time interval from $t - \tau$ to t, at which time it comes back to the atomic core (i.e., the return time is τ). The electron then recombines with the atomic core, exchanging n photons with the laser field and emitting an x-ray photon having wave vector $\mathbf{K}'$ and energy $\hbar\omega_{\mathbf{K}'}$. The matrix element $T^{(+)}_{\mathbf{K},\mathbf{K}'}(n)$ describes the process in which the x-ray photon having wave vector $\mathbf{K}'$ and energy $\hbar\omega_{\mathbf{K}'}$, is emitted first. It was shown in paper [17] that the contribution of $T^{(+)}_{\mathbf{K},\mathbf{K}'}(n)$ to the DCS can be neglected in comparison to the contribution of $T^{(-)}_{\mathbf{K}',\mathbf{K}}(n)$ (for $|n| > 5$). This is in agreement with the three-step model described in Section II (cf. Fig. 2). The three-dimensional integral over the intermediate electron momenta in (9) can be carried out using the time-dependent WBK approximation [17]. The integral over the return time τ is computed numerically, and, finally,

the T matrices, (8), are obtained using the fast Fourier transform method. The explicit analytical forms of the matrix elements in (9) for the H atom are given in [17] in terms of the vector potential $\mathbf{A}(t)$, the stationary momentum $\hbar\mathbf{q}_s \equiv \hbar\mathbf{q}_s(t, \tau) = -\frac{e}{\tau}\int_{t-\tau}^{t} dt' \mathbf{A}(t')$ and the action $S_s \equiv S(\mathbf{q}_s; t, \tau)$. The expressions for $\mathbf{A}(t)$, $\mathbf{q}_s$, and S_s in the presence of a static electric field are given in [18].

In order to further analyze plateau structures, observed in [17, 18], in Figs. 6 and 7 we present numerical results for the DCS for laser-assisted x-ray-hydrogen atom scattering (in units of r_e^2, where $r_e = 2.8 \times 10^{-15}$ m is the classical electron radius) as functions of the number of photons n exchanged with the Nd : YAG laser field ($\hbar\omega$ = 1.17 eV). The laser field intensity is $I = i \times 10^{14}$ W/cm^2, $i = 1, \ldots, 5$, the incident x-ray photon energy is $\hbar\omega_\mathbf{K} = j\hbar\omega$, where j = (a) 15, (b) 31, and (c) 61, and the static electric field strength is $E_S = 0$ (Fig. 6) and E_S = 2 MV/cm (Fig. 7). The main characteristics of the DCS in the absence of a static electric field (Fig. 6) are the following: (i) an extended plateau for positive values of n appears as the laser field intensity increases, (ii) this plateau is more extended for lower values of the incident x-ray photon energies, (iii) the cutoff positions (denoted by c, where $n_{\max}\hbar\omega = cU_p$) tend to the HHG cutoff position (c = 3.17) as the laser field intensity increases and as the incident x-ray photon energies decrease, (iv) for $\omega_\mathbf{K} = 15\omega$ there is a sharp maximum for elastic scattering and the negative n plateau is absent; with increase of $\omega_\mathbf{K}$ the maximum for small values of $|n|$ is less sharp and a negative n plateau appears and becomes longer, (v) for low laser field intensities, the positive n plateau is absent (cf. $i = 1$ in Fig. 6b, and $i = 1, 2$ in Fig. 6c) and the height of the negative n plateau is lower, i.e., the DCS is smaller (cf. $i = 1$ in Fig. 6c).

The main additional features of the DCS in the presence of a static electric field (Fig. 7) are: (i) a second positive n plateau appears, having orders of magnitude smaller DCS, but which is one order of magnitude longer in n, (ii) the dependence of the cutoff position of this second plateau on the laser field intensity and on the incident x-ray photon energy is in agreement with the results of classical analysis (cf. Fig. 5): with the increase of I the parameter d, where $n_{\max,2}\hbar\omega = dU_p$, decreases, and the limiting value of d is equal to the corresponding value for HHG in the presence of a static field; contrary to the behavior of c, d increases with increase of $\omega_\mathbf{K}$, (iii) the behavior of the cutoff position of the shorter positive n and larger DCS plateau is also in agreement with the results of Fig. 5 and is very similar to that in the absence of the static field: compare the corresponding values of c in Figs. 6 and 7.

These numerical results, both with and without a static electric field, confirm the predictions of the three-step model. Moreover, a simple classical analysis predicts very well quantum-mechanical numerical values of the DCS plateau and cutoff positions. The relative height of the plateaus can be estimated considering the values of the return time τ which correspond to these cutoffs (cf. Fig. 4). Namely, because the T-matrix elements contain a term proportional to $\tau^{-3/2}$ [17], the DCS decreases with increase of τ. Physically, this corresponds to the spreading of the electron wave packet. This explains why the second positive n plateau in Fig. 7 has a smaller DCS. It should also be mentioned that the semiclassical analysis of the T-matrix elements [17, 18] leads to the same results as the classical analysis, presented in Section III in the present paper.

V. HARMONIC EMISSION RATES IN PARALLEL STATIC MAGNETIC AND ELECTRIC FIELDS

The rate of emission of a harmonic photon of frequency $\Omega = cK$ and polarization $\mathbf{e}_\Omega$ into a solid angle $d\hat{\mathbf{n}}_\mathbf{K}$ is [22]

$$w_{fi}(\Omega, \mathbf{e}_\Omega) = \frac{dR_{fi}(\Omega, \mathbf{e}_\Omega)}{d\hat{\mathbf{n}}_\mathbf{K}} = \frac{\Omega^3}{8\pi^2\varepsilon_0\hbar c^3}|T_{fi}(n)|^2, \quad \hbar\Omega + E_f = n\hbar\omega + E_i, \tag{10}$$

where n is the number of photons exchanged with the laser field during the transition from the initial atomic state with the energy E_i to the final atomic state with the energy E_f, and the T-matrix element is

$$T_{fi}(n) = \int_0^T \frac{dt}{T}\langle\Phi_f^{(-)}(t)|e\mathbf{r}\cdot\mathbf{e}_\Omega^*|\Phi_i^{(+)}(t)\rangle\exp(i\Omega t), \quad T = \frac{2\pi}{\omega}. \tag{11}$$

The states $|\Phi_j^{(\pm)}(t)\rangle$, $j = i, f$, are the solutions of the Schrödinger equation for the system (atom + laser field + static fields) with the appropriate boundary conditions: the state $|\Phi_i^{(+)}(t)\rangle(|\Phi_f^{(-)}(t)\rangle)$ evolves from the initial (final) atomic state $|u(t')\rangle$, $t' \longrightarrow -\infty$ ($t' \longrightarrow +\infty$), under the action of the total Green's operator $G^{(+)}(t, t')$ ($G^{(-)}(t, t')$). For the HHG process both the initial and final states are usually the atomic ground state $|u(t)\rangle = |u_0\rangle\exp(iI_p t/\hbar)$ so that we can omit the indexes i and f. Furthermore, we will adopt here a slightly different approach for computing the harmonic emission rate. Namely, the quantity which enters the classical Maxwell equations as a source is the dipole-moment expectation value [20, 25]

$$\mathbf{d}(t) = \langle\Phi^{(+)}(t)|e\mathbf{r}|\Phi^{(+)}(t)\rangle. \tag{12}$$

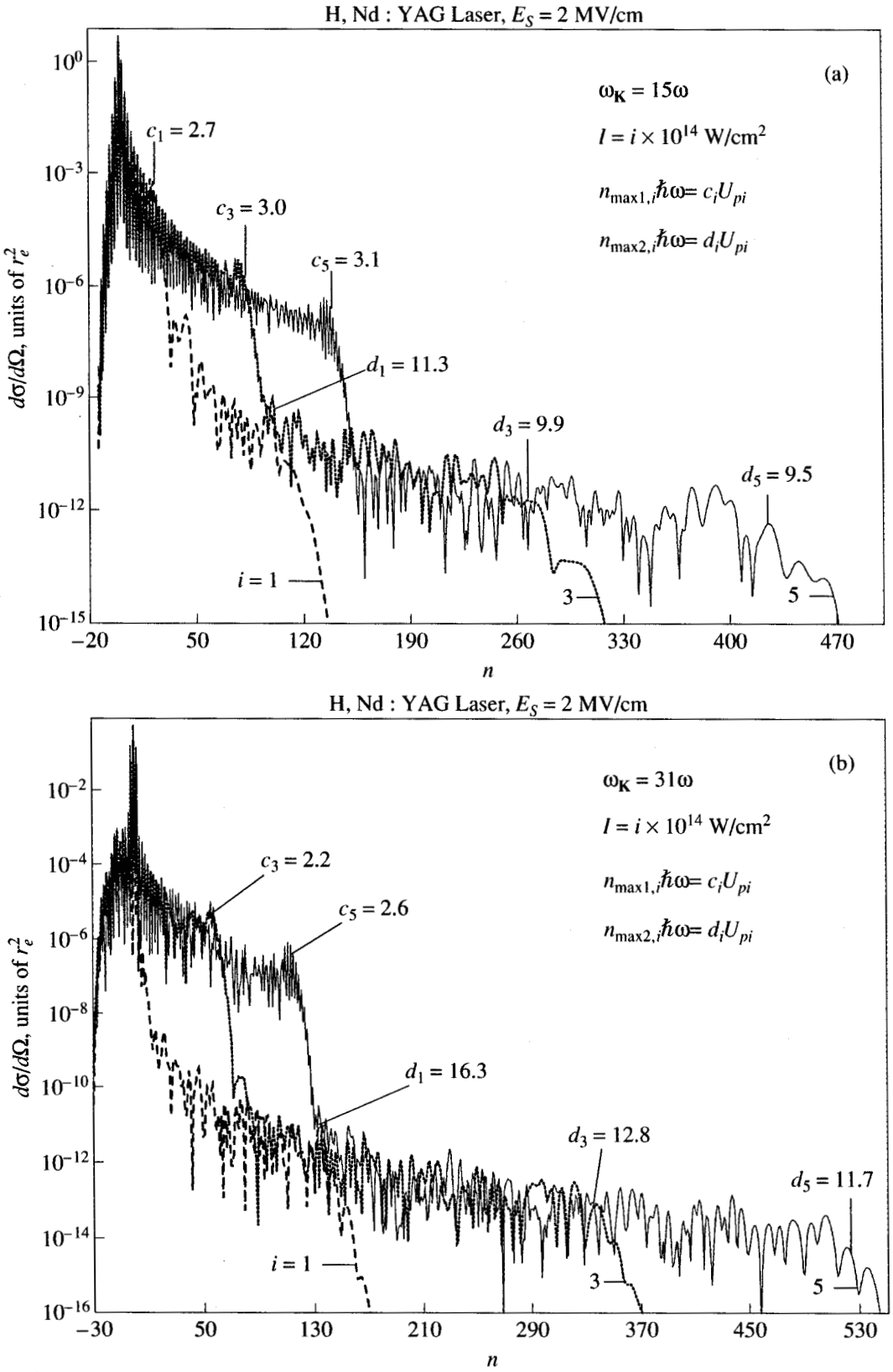

Fig. 7. The same as in Fig. 6, but in the presence of an additional static electric field having strength $E_S = 2$ MV/cm, and for laser intensities $I(i) = i \times 10^{14}$ W/cm^2, where $i = 1$, 3, and 5. The energy cutoff positions for higher and lower DCS plateaus are denoted by the ponderomotive energy multiples c_i and d_i, respectively.

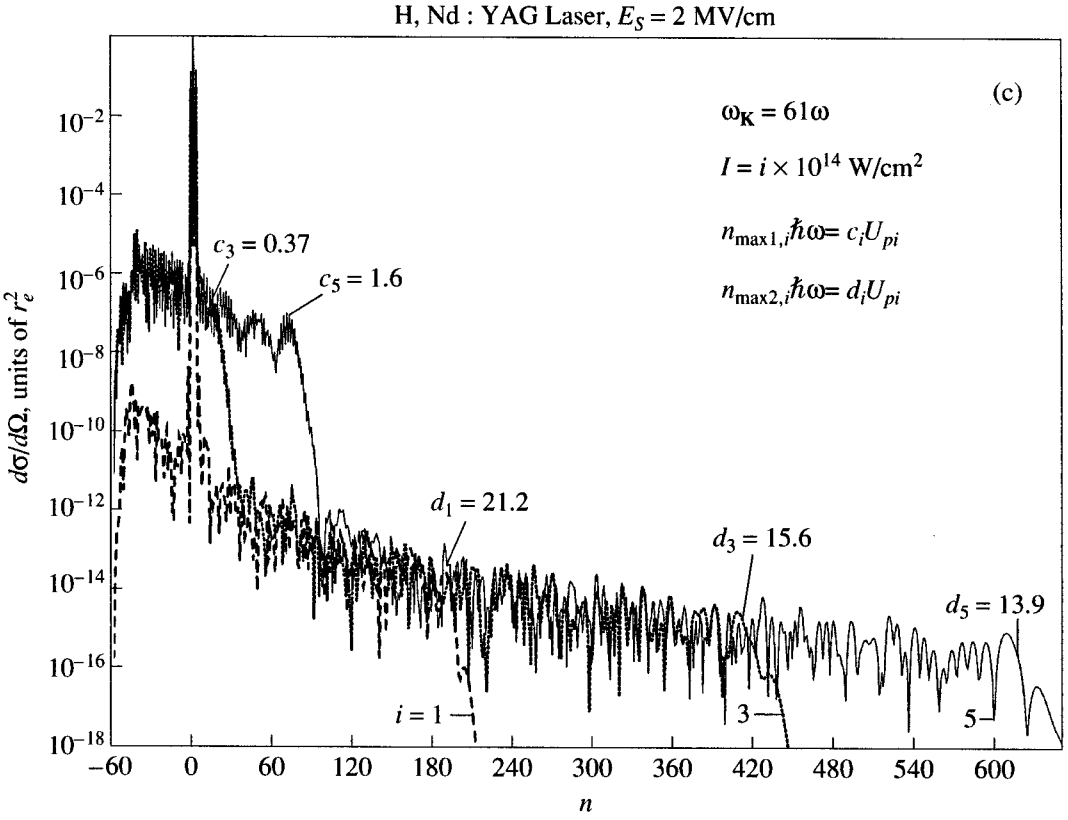

Fig. 7. (Contd.)

Therefore, instead of (10) and (11), we calculate the emission rate of the nth harmonic ($\Omega = n\omega$) according to

$$w_n = \frac{n^3\omega^3}{8\pi^2\varepsilon_0\hbar c^3}|\mathbf{D}_n \cdot \mathbf{e}_\Omega^*|^2,$$
$$\mathbf{D}_n = \int_0^T \frac{dt}{T}\mathbf{d}(t)\exp(in\omega t). \quad (13)$$

Using the strong-field approximation and neglecting the continuum-continuum coupling, the time-dependent dipole can be written as [20]

$$\mathbf{d}(t) = \int_{t_0}^{t} dt' \langle u(t)|e\mathbf{r}G_L(t, t')e\mathbf{E}_L(t') \cdot \mathbf{r}|u(t')\rangle + \text{c.c.}, \quad (14)$$

where $G_L(t, t')$ is the Volkov-type Green's operator for the electron in the presence of the laser field and the static fields, and $e\mathbf{E}_L(t') \cdot \mathbf{r}$ is the interaction of the electron with the laser field in the length gauge. We suppose that the static fields are not strong enough to modify the atomic ground state $|u(t)\rangle$. However, these fields are included in $G_L(t, t')$ so that they influence the intermediate states of the electron. In the case of a linearly polarized laser field and parallel static electric and magnetic fields, we compute the dipole moment $D_n = (1/T)\int_0^T dt\, d(t)\exp(in\omega t)$, where, according to (14) and the results of [26],

$$d(t) = \frac{-ie^2}{\hbar}\int_{-\infty}^{t} dt' E_L(t') \int_{-\infty}^{\infty} dq \sum_{\nu,\mu} \langle u_0|z|\nu\mu Q(t)\rangle$$
$$\times \langle \nu\mu Q(t')|z|u_0\rangle \exp\left[-\frac{i}{\hbar}S_{\nu\mu}(q; t, t')\right] + \text{c.c.}, \quad (15)$$

with

$$Q(t) = q + \frac{e}{\hbar}[A_L(t) + A_S(t)],$$
$$S_{\nu\mu}(q; t, t') = \int_{t'}^{t} dt'' \frac{\hbar^2}{2m}\left\{q + \frac{e}{\hbar}[A_L(t'') + A_S(t'')]\right\}^2$$
$$+ (I_p + E_{\nu\mu})(t - t') = \hbar q[\alpha(t) - \alpha(t')]$$
$$+ U(t) - U(t') + \left(\frac{\hbar^2 q^2}{2m} + I_p + E_{\nu\mu}\right)(t - t'), \quad (16)$$
$$\alpha(t) = \frac{e}{m}\int^{t} dt'[A_L(t') + A_S(t')],$$

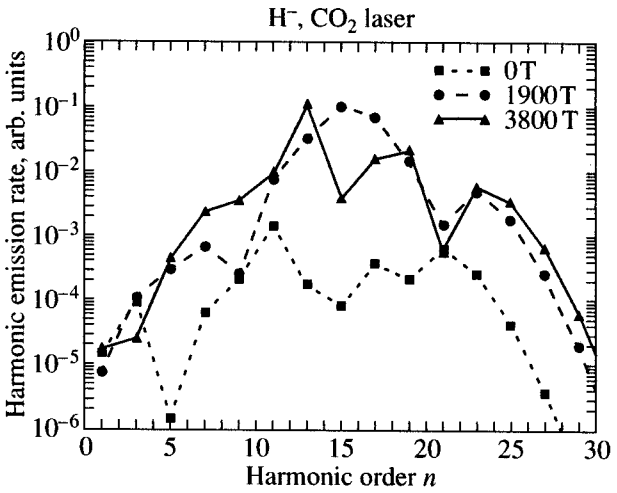

Fig. 8. Harmonic emission rates as functions of the harmonic order n for the H^- ion and a CO_2 laser with intensity $I = 5 \times 10^{10}$ W/cm^2. The magnetic field induction is: $B = 0$ T (squares), 1900 T (circles), and 3800 T (triangles).

$$U(t) = \frac{e^2}{2m}\int^t dt'[A_L(t') + A_S(t')]^2,$$

$$E_{\nu\mu} = \left[\nu + \frac{1}{2}(|\mu| + \mu + 1)\right]\hbar\omega_B, \quad \omega_B = \frac{eB}{m}.$$

The method of computation of the matrix elements with the wavefunctions $\langle\rho\phi z|\nu\mu q\rangle \equiv \Psi_{\nu\mu q}(\rho, \phi, z, 0)$ is given in the appendices of [26]. The integral over the z-component of the intermediate electron momentum $\hbar q$ is computed using the saddle-point method, as in [4, 20]. This gives the factor $[2\pi m\hbar/(i\tau)]^{1/2}\exp[-iS_s(t, \tau)/\hbar]$, where $S_s(t, \tau) \equiv S_{\nu\mu}(q_s; t, t-\tau)$ is the stationary action, and $\hbar q_s$ is the stationary momentum

$$\begin{aligned}\hbar q_s(t, \tau) &= -\frac{e}{\tau}\int_{t-\tau}^{t} dt''[A_L(t'') + A_S(t'')] \\ &= \frac{m}{\tau}[\alpha(t-\tau) - \alpha(t)], \\ \tau &= t - t'.\end{aligned} \tag{17}$$

The final result for the time-dependent dipole is [26]

$$\begin{aligned}d(t) = -ie^2\left(\frac{2\pi m}{i\hbar^3}\right)^{1/2}\int_0^\infty \frac{d\tau}{\tau^{1/2}}E_L(t-\tau) \\ \times\sum_{\nu,\mu}\langle u_0|z|\nu\mu Q_s(t)\rangle\langle\nu\mu Q_s(t-\tau)|z|u_0\rangle \\ \times\exp\left[-\frac{i}{\hbar}S_s(t, \tau)\right] + \text{c.c.}\end{aligned} \tag{18}$$

The summation over the quantum numbers ν and μ can be performed analytically, and, as the result for the

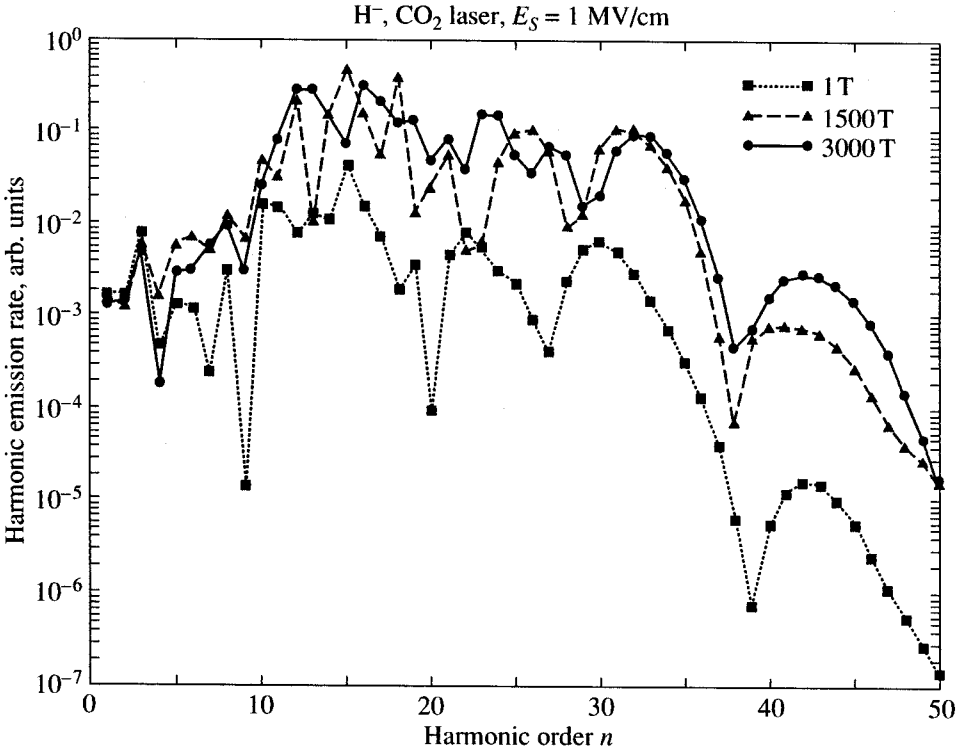

Fig. 9. The same as in Fig. 8, but in the presence of a parallel static electric field having strength $E_S = 1$ MV/cm, and for the following values of the magnetic field induction: $B = 1$ T (squares), 1500 T (triangles), and 3000 T (circles).

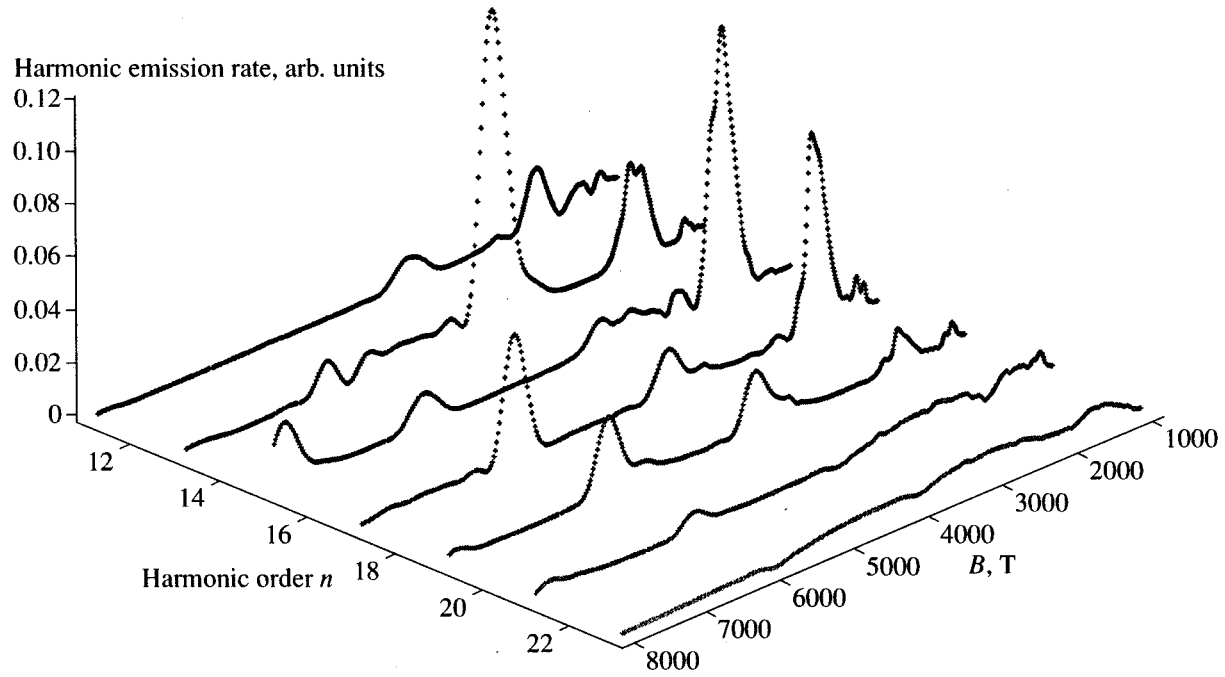

Fig. 10. Harmonic emission rates (in arbitrary units) as functions of the harmonic order n and of the magnetic field induction B. The laser field and the H^- ion parameters are as in Fig. 8.

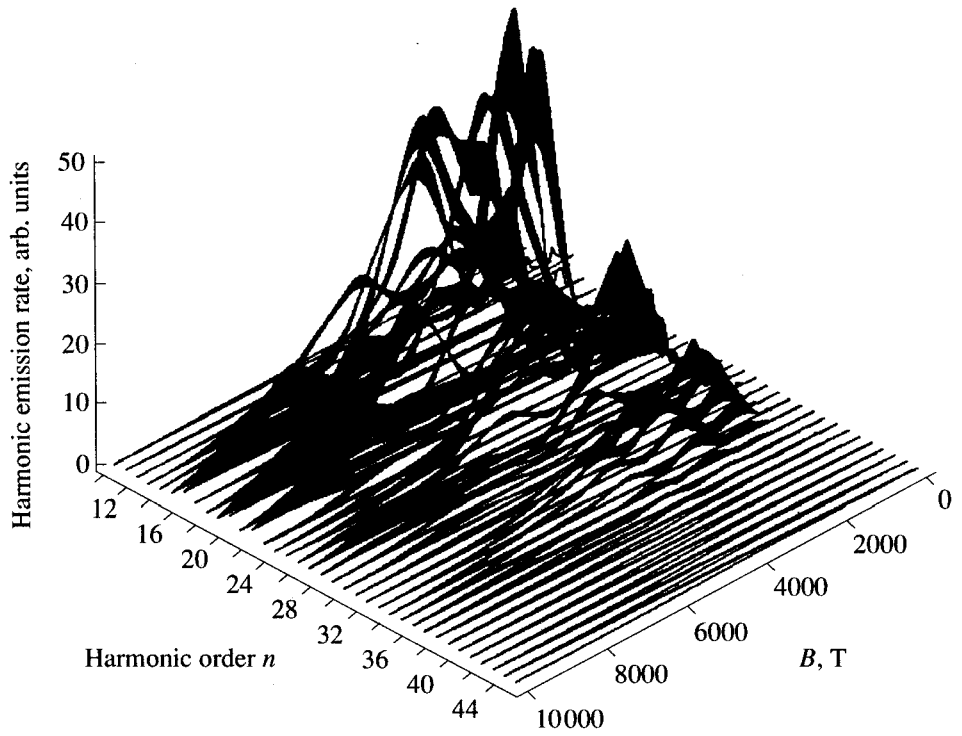

Fig. 11. The same as in Fig. 10, but in the presence of a parallel static electric field having strength $E_S = 1$ MV/cm.

summed product of the matrix elements in (18), we obtained a single integral over a function which contains exponential integral functions. This integral can be computed efficiently using the method described in [26].

We present numerical results for the harmonic emission rates for the H^- ion and a CO_2 laser with intensity $I = 5 \times 10^{10}$ W/cm^2, both with and without a static electric field having strength $E_S = 1$ MV/cm, and for differ-

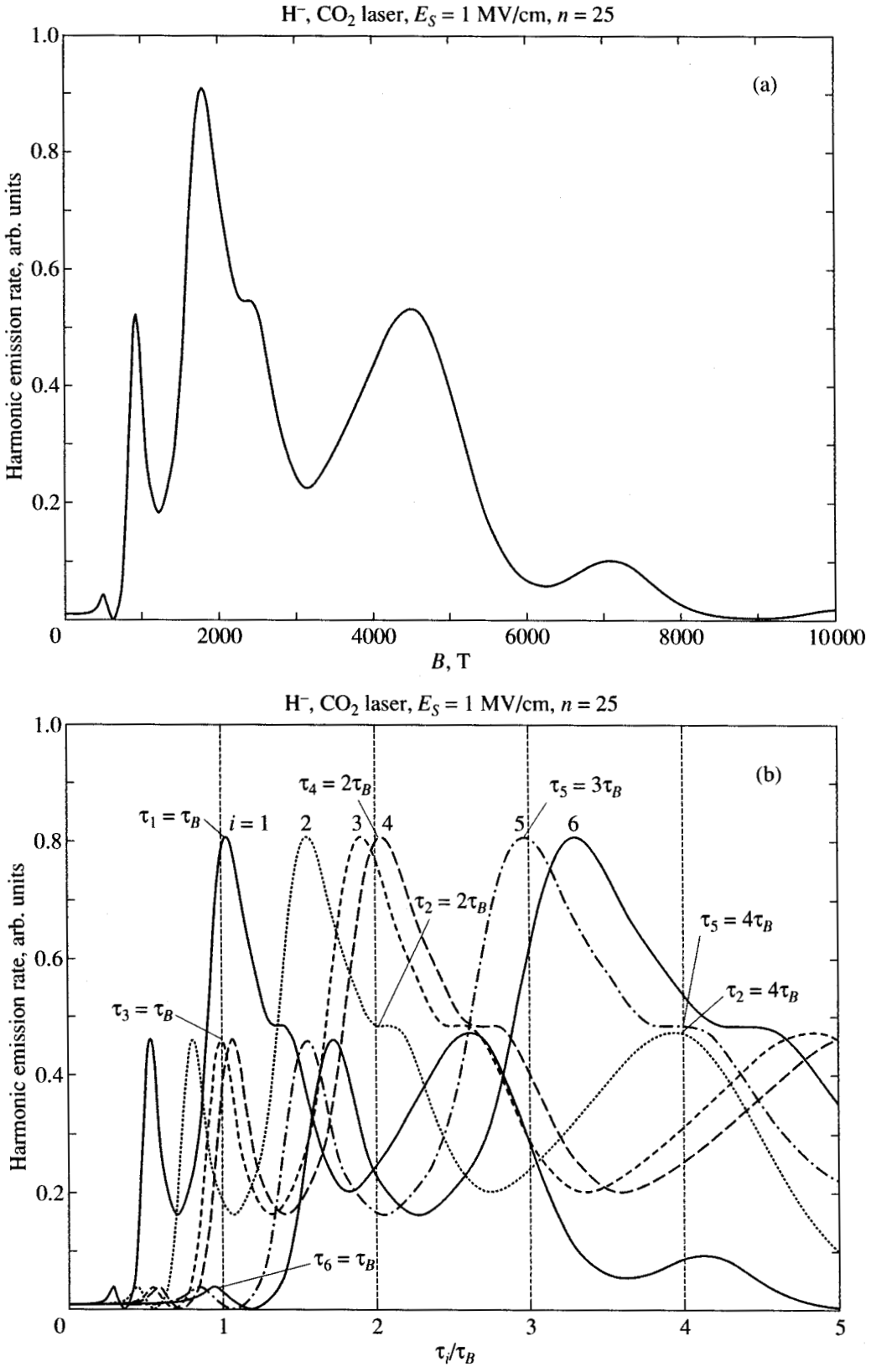

Fig. 12. The 25th harmonic emission rate as a function of the magnetic field induction B for the same parameters as in Fig. 11. (a) Emission rate plotted vs. $B(\tau)$. (b) Emission rate plotted vs. the dimensionless parameters τ_i/τ_B, $i = 1, \ldots, 6$, where τ_i is the ith classical return time. The harmonic emission rate has maxima for $\tau_i = j\tau_B$, where i and j are integers, and τ_B is the cyclotron period.

ent values of the magnetic induction B (cf. Fig. 3 for our classical analysis for the case of $B = 0$). In Fig. 8 we present the emission rates as functions of the harmonic order n for $E_S = 0$ and for $B = 0$ T (squares), 1900 T (circles), and 3800 T (triangles). The classical cutoff position is $3.17U_p + I_p = 20.9\hbar\omega$, so that $n_{max}(B = 0) \approx 21$, which agrees with the results in Fig. 8. In the presence of a magnetic field, the cutoff energies are increased by the ground-state Landau level energy $\hbar\omega_B/2 = e\hbar B/(2m)$, which is $0.944\hbar\omega$ and $1.89\hbar\omega$ for $B = 1900$ T and 3800 T, respectively. In absence of a static electric field, only the odd harmonics can be generated, so that the cutoff position is $n_{max} \approx 23$ both for $B = 1900$ T and 3800 T. For $B = 1900$ T there is a pronounced maximum of the harmonic emission rate for $n = 15$, while for $B = 3800$ T the maximum is at $n = 13$.

In Fig. 9 we present the emission rates as functions of the harmonic order n similarly as in Fig. 8, but for $E_S = 1$ MV/cm and for $B = 1$ T (squares), 1500 T (circles), and 3000 T (triangles). The static electric field breaks the symmetry of the system and emission rates for both odd and even harmonics are of comparable magnitude. The harmonic spectrum is also extended to higher harmonic orders. Two additional cutoffs appear, one at the 31st and the other at the 43rd harmonic, which agrees with the results of our classical analysis in Section III (cf. Fig. 3). As in Fig. 8, the emission rates for particular harmonics are increased by more than two orders of magnitude in the presence of the magnetic field. It is important to note that, by choosing particular values of both fields, it is possible to generate higher-order harmonics having higher emission rates.

In order to explore the dependence of the harmonic emission rates on the magnetic field strength, in Figs. 10 and 11 we present the rates (in arbitrary units on a linear ordinate scale) as functions of the harmonic order n and of the magnetic induction B. The results presented in Fig. 10 (for $E_S = 0$) show pronounced maxima for particular values of B. One notices also a periodicity in the appearance of these maxima. In [11] we referred to this periodicity as revivals of the harmonic emission rates. The physical explanation of these revivals follows from the three-step model. We expect that the rates have maxima if the electron (or, quantum mechanically speaking, its wave packet) returns to the origin both in the perpendicular and the parallel directions at the same time. As we mentioned in the section concerning our classical analysis, the electron returns to the origin at time $t_1 = t_0 + \tau_B, t_0 + 2\tau_B, \ldots$, if the condition $z(t_1) = 0$ is fulfilled. Therefore, we expect maximal rates for values of B for which an integer multiple of τ_B is equal to the return time of the laser field-driven (and, if present, static electric field-driven) ionized electron wave packet to the nucleus, i.e., for $j\tau_B = t_1 - t_0 = \tau$, $j = 1, 2, \ldots$. In [11] such a physical explanation was supported by presenting $|D_n|^2$ vs. B in terms of $\tau_i(n)/\tau_B = [e\tau_i(n)/(2\pi m)]B$, where $\tau_i(n)$ is the return time, which corresponds to the ith return of the electron having energy $n\hbar\omega - I_p$ to the origin (see the intersection of the horizontal lines for a fixed n and the dot-dashed curve, obtained from the condition $z(t_1) = 0$, in Fig. 3). The results presented in [11] have shown that, whenever $\tau_i(n)$ is close to an integer multiple of τ_B, there is a revival of the intensity of the emitted harmonics; moreover the interval between revivals is approximately τ_B. In Fig. 11 we present the harmonic emission rates as in Fig. 10, but for $E_S = 1$ MV/cm. The B-dependence of the rates is now more complex. We still have maxima for particular values of B, but they are broader and interference structures are present. In order to explain the appearance of these maxima using the classical analysis of Section III, we consider, as an example, one particular harmonic. In Fig. 12a we present the 25th harmonic emission rate as a function of the magnetic induction B for the same atomic, laser and static E and B field parameters as in Fig. 11. For some particular values of B, the emission rate has maxima, but these maxima are broader and are not equally spaced, as in the absence of the static electric field. Nevertheless, this behavior can be explained using our classical analysis. From Fig. 3 one can see that the horizontal line $n = 25$ has six intersections with the full and dotted curves which are obtained from the condition that the electron returns to the origin. We denote the corresponding return times by τ_i, $i = 1, \ldots, 6$. In Fig. 12b we present the rates for the same parameters as in Fig. 12a, but as functions of the dimensionless parameter τ_i/τ_B. We have six curves denoted by $i = 1, \ldots, 6$. The position of the highest maximum is at $\tau_1 = \tau_B$, which indicates that the rate has the highest maximum when the shortest electron return time in the parallel direction is equal to one cyclotron period. The origins of other maxima can be identified in a similar way and are denoted in Fig. 12b. Even the lowest maximum position ($\tau_6 = \tau_B$) can be satisfactorily explained. A similar analysis can be done for other harmonics. Thus, our quantum-mechanical results confirm the three-step model for harmonic generation in the presence of strong static electric and magnetic fields as well as its applicability to laser-assisted XAS.

CONCLUSION

We have shown that it is possible to control HHG and XAS in a linearly polarized laser field by adding parallel static electric and magnetic fields. Using a simple classical analysis, based on the three-step model, we predicted the main characteristic of these processes, i.e., the positions of the plateaus and the cutoffs for the DCS of laser-assisted XAS and for the harmonic emission rates as functions of the number of photons exchanged with the laser field. Our quantum-mechani-

cal results confirm these predictions. We have also shown a clear connection between the laser-assisted XAS and HHG. In the high laser field intensity limit, the cutoff position for laser-assisted XAS approaches the cutoff positions of HHG from below (i.e., from lower energies). If a static electric field is present, both high- and low-energy plateaus appear. It is important to note that, in the high laser field intensity limit, the XAS cutoff position of the high-energy plateau approaches the cutoff position for HHG from above. This enables control of the scattered x-ray's energy by choosing proper values of the laser field intensity and the static electric field strength. It is possible to produce the scattered x-rays having an order of magnitude higher energy than the incident x-rays (with the extra energy being absorbed from the laser field). We have also considered the influence of a parallel magnetic field on the HHG process. It was shown that the magnetic field can considerably increase the harmonic emission rate and that there are optimal values of the magnetic induction for which the rate for a particular harmonic has a maximum. We have also explained, using the classical three-step model, that the positions of these maxima correspond to such values of magnetic induction for which an integer multiple of the classical period for motion perpendicular to the magnetic field is equal to the return time of the laser field-driven and static electric field-driven ionized electron wave packet to the nucleus. We interpret this fact to mean that the harmonic emission rate has a maximum if the electronic wave packet is at the nucleus both in the parallel and in the perpendicular directions at the same time. While the static magnetic field (for the inductions we are considering) only slightly affects the position of the cutoff, the static electric field can introduce new plateaus with their own cutoffs. A properly chosen combination of the static electric and magnetic fields can both increase the harmonic emission rate and shift the cutoff position to a higher harmonic order.

ACKNOWLEDGMENTS

This work has been supported in part by the U.S. National Science Foundation under Grant No. PHY-9722110. D.M. is also supported by the Alexander von Humboldt Foundation.

REFERENCES

1. Salières, P., L'Huillier, A., Antoine, Ph., and Lewenstein, M., 1999, *Adv. At. Mol. Opt. Phys.*, **41**, 83; Protopapas, M., Keitel, C.H., and Knight, P.L., 1997, *Rep. Prog. Phys.*, **60**, 389; and references therein.
2. Spielmann, Ch., Burnett, N.H., Sartania, S., *et al.*, 1997, *Science*, **278**, 661.
3. Long, S., Becker, W., and McIver, J.K., 1995, *Phys. Rev. A*, **52**, 2262; Figueira de Morisson Faria, C., Becker, W., Dörr, M., and Sandner, W., 1999, *Laser Phys.*, **9**, 388.
4. Milošević, D.B. and Piraux, B., 1996, *Phys. Rev. A*, **54**, 1522; Gaarde, M.B., L'Huillier, A., and Lewenstein, M., 1996, *Phys. Rev. A*, **54**, 4236.
5. Ivanov, M., Corkum, P.B., Zuo, T., and Bandrauk, A., 1995, *Phys. Rev. Lett.*, **74**, 2933; Antoine, Ph., Piraux, B., Milošević, D.B., and Gajda, M., 1996, *Phys. Rev. A*, **54**, R1761; Antoine, Ph., Milošević, D.B., Gaarde, M.B., *et al.*, 1997, *Phys. Rev. A*, **56**, 4960.
6. De Bohan, A., Antoine, Ph, Milošević, D.B., and Piraux, B., 1998, *Phys. Rev. Lett.*, **81**, 1837.
7. Bao, M.Q. and Starace, A.F., 1996, *Phys. Rev. A*, **53**, R3723.
8. Lohr, A., Becker, W., and Kleber, M., 1997, *Laser Phys.*, **7**, 615.
9. Wang, B., Li, X., and Fu, P., 1998, *J. Phys. B*, **31**, 1961.
10. Zuo, T., Bandrauk, A., Ivanov, M., and Corkum, P.B., 1995, *Phys. Rev. A*, **51**, 3991; Zuo, T. and Bandrauk, A.D., 1995, *J. Nonl. Opt. Phys. Mat.*, **4**, 533; Bandrauk, A.D., Ruel, J., Zuo, T., and Yu, H., 1997, *Int. J. Quant. Chem.*, **64**, 613.
11. Milošević, D.B. and Starace, A.F., 1999, *Phys. Rev. Lett.*, **82**, 2653.
12. Preston, S.G., Sanpera, A., Zepf, M., *et al.*, 1996, *Phys. Rev. A*, **53**, R31.
13. Kopold, R., Becker, W., and Kleber, M., 1998, *Phys. Rev. A*, **58**, 4022.
14. Bandrauk, A.D. and Yu, H., 1999, *Phys. Rev. A*, **59**, 539.
15. Donnelly, T.D., Ditmire, T., Neuman, K., *et al.*, 1996, *Phys. Rev. Lett.*, **76**, 2472.
16. Watson, J.B., Sanpera, A., Chen, X., and Burnett, K., 1996, *Phys. Rev. A*, **53**, R1962; Sanpera, A., Watson, J.B., Lewenstein, M., and Burnett, K., 1996, *Phys. Rev. A*, **54**, 4320; De Luca, S. and Fiordilino, E., 1996, *J. Phys. B*, **29**, 3227; Jarque, E.C., and Plaja, L., 1998, *J. Phys. B*, **31**, 1687.
17. Milošević, D.B. and Ehlotzky, F., 1998, *Phys. Rev. A*, **58**, 2319.
18. Milošević, D.B. and Starace, A.F., 1998, *Phys. Rev. Lett.*, **81**, 5097.
19. Kuchiev, M.Yu., 1987, *Pis'ma Zh. Eksp. Teor. Fiz.*, **45**, 319 (*JETP Lett.*, **45** (7), 404); Kulander, K.C., Schafer, K.J., and Krause, J.L., 1993, in *Proc. of the SILAP Conf.*, Piraux, B. *et al.*, Eds. (New York: Plenum, p. 95); Corkum, P.B., 1993, *Phys. Rev. Lett.*, **71**, 1994.
20. L'Huillier, A., Lewenstein, M., Salières, P., *et al.*, 1993, *Phys. Rev. A*, **48**, R3433; Lewenstein, M., Balcou, Ph., Ivanov, M.Yu., *et al.*, 1994, *Phys. Rev. A*, **49**, 2117.
21. Heitler, W., 1954, *The Quantum Theory of Radiation* (Oxford: Clarendon).
22. Loudon, R., 1983, *The Quantum Theory of Light* (Oxford: Clarendon).
23. Levinger, J.S., 1952, *Phys. Rev.*, **87**, 656.
24. Jung, M., Dunford, R.W., Gemmell, D.S., *et al.*, 1998, *Phys. Rev. Lett.*, **81**, 1596.
25. Becker, W., Lohr, A., Kleber, M., and Lewenstein, M., 1997, *Phys. Rev. A*, **56**, 645.
26. Milošević, D.B. and Starace, A.F., 1999, *Phys. Rev. A*, **60**, 3160.